13th ewtec 2019
Proceedings of the 13th European Wave and Tidal Energy Conference 1-6 Sept 2019, Naples, Italy

# Preliminary results from a scaled test of arrays of point-absorbers with 6 DOF

Marianna Giassi, Simon Thomas, Zahra Shahroozi, Jens Engström, Jan Isberg, Tom Tosdevin, Martyn Hann, and Malin Göteman

***Abstract*—If realized in offshore commercial installations, most wave energy technologies will likely be deployed in parks consisting of many devices. Different analytical and numerical methods and optimization algorithms exist to predict and optimize the total performance of wave energy parks, but so far few experimental tests have been carried out and there is very little available data to validate the simulations. In this paper, preliminary results from wave energy array experiments in scale 1:10 are presented. The experiments were carried out in the COAST laboratory of Plymouth University, UK, with six identical point-absorber wave energy converters. The devices consist of a floating ellipsoid buoy, free to move in all six degrees of freedom, connected to a rotating power take-off system situated at a gantry above the water. We show preliminary results of power absorption for three different arrays configurations, as well as the power absorption from each individual device inside the layouts; also, the wave elevation in the basin has been analysed and its reduction due to the presence of the wave power farm computed.**

***Index Terms*—Wave energy, arrays, experiments, wave tank, scale test, point absorber, park optimization.**

## I. Introduction

FOR most wave energy concepts, a large-scale electricity production requires that the wave energy converters (WECs) are deployed in arrays of multiple units. In particular, this is true for point-absorbing WECs, such as the wave energy device developed at Uppsala University, Sweden [1]. The deployment in arrays, or parks, is also required to share and thus lower the costs of the produced electricity, as well as to lower the fluctuations in the power delivered to the grid [2]. The WECs in an array will interact hydrodynamically by scattered and radiated waves, and the full performance of the array is affected by a large number of parameters such as the array layout, number of devices and their separation distance, and the wave climate. At the present stage of the research, developers need to rely on simulations tools in order to predict the power output of the park and to optimize these design variables, but there is very little experimental data available to validate the numerical modelling tools. An array consisting of four Wavebob models in scale 1:19 was studied experimentally and compared to a numerical time-domain model in [3]. Three floating oscillating water column devices were studied experimentally in [4] and compared to semi-analytical results based on the multiple scattering method. Similarly, experimental results from three floating oscillating water column devices of spar buoy type in scale 1:32 were presented in [5] and compared to the case of an isolated device. Numerical simulations as well as experimental results for five WaveStar devices in scale 1:20 were presented in [6]. The power take-off (PTO) consisted of a piston driven by an electric motor to model a linear damper. The simulations were carried out using the software NEMOH combined with a direct matrix method, and showed good agreement with the experimental data.

In the mentioned works [3]–[6], only one array layout was studied for each test, based on a staggered park geometry or WECs in a row. Several layouts of arrays with up to 25 heaving point-absorber buoys connected to friction damping PTOs were studied in the experimental campain presented in [7]–[9]. The performance was studied in different regular and irregular short- and long-crested waves, and up to 18% reduction of the wave height due to park effects were found. Results from a similar experimental set-up was presented in [10], where different array layouts with 24 heaving buoys were studied and compared to three different numerical models, and it was found that the park interactions could imply up to 26% energy loss for the total park.

For point-absorbing WECs with buoys free to move in all six degrees of freedom, so far no array experiments have been published. This paper present preliminary results from experiments of an array of point absorber WECs conducted in the COAST Lab at Plymouth University, UK. The experimental set-up consist of six identical ellipsoidal floaters moving in six degrees of freedom and connected via ropes and pulleys to six power take-off systems (PTO) located outside the water. The model represents a 1:10 scaled prototype of an array of point absorber composed by a 5 m buoy installed at 25 m depth,

Paper ID number: 1412, thematic track: Wave device development and testing (WDD). This research is supported by the the Swedish Research Council (VR, grant number 2015-04657), the Swedish Energy Agency (project number 40421-1), and StandUp for Energy.

M. Giassi is with the Department of Engineering Science, Uppsala University, Box 534, 751 21 Uppsala, Sweden (e-mail: marianna.giassi@angstrom.uu.se).

S. Thomas is with the Department of Engineering Science, Uppsala University, Box 534, 751 21 Uppsala, Sweden (e-mail: simon.thomas@angstrom.uu.se).

Z. Shahroozi is with the Department of Engineering Science, Uppsala University, Box 534, 751 21 Uppsala, Sweden (e-mail: Zahra.Shahroozi.5479@student.uu.se).

J. Engström is with the Department of Engineering Science, Uppsala University, Box 534, 751 21 Uppsala, Sweden (e-mail: jens.engstrom@angstrom.uu.se).

J. Isberg is with the Department of Engineering Science, Uppsala University, Box 534, 751 21 Uppsala, Sweden (e-mail: jan.isberg@angstrom.uu.se).

T. Tosdevin is with the School of Marine Science and Engineering, University of Plymouth, Plymouth, Devon PL4 8AA, UK (e-mail: tom.tosdevin@postgrad.plymouth.ac.uk).

M. Hann is with the School of Marine Science and Engineering, University of Plymouth, Plymouth, Devon PL4 8AA, UK (e-mail: martyn.hann@plymouth.ac.uk).

M. Göteman is with the Department of Engineering Science, Uppsala University, Box 534, 751 21 Uppsala, Sweden (e-mail: malin.goteman@angstrom.uu.se).

  

based on the WEC concept developed at Uppsala University, Sweden [1].

The full goal of the experiment consists of studying the performance of different array layouts and compare the results with earlier optimization simulations performed with genetic algorithms [11], and also to study the performance using different control algorithms. In this paper, the focus is the description of the physical setup and the presentation of some preliminary results in terms of measurements of the wave elevation in the tank and energy absorbtion for three different arrays configurations. The PTO is performed by passive damping using a rotatory system appositely designed for the wave tank experiment, described in details in [12]. Different regular and irregular unidirectional waves have been tested.

The paper is organized as follows. The WEC model, the experimental set-up and the wave parameters are described in section II. The results of the experiments are presented in section III. Conclusions of the study are presented in section IV.

## II. Method

### A. Physical model

The WEC model is based on the point-absorber wave energy concept developed at Uppsala University [1]. In the full-scale device, each floating buoy is connected via a line to a linear generator at the seabed, and the generated electricity is then transmitted to shore via a substation.

Here, six WEC models in scale 1:10 are used, each consisting of an ellipsoid polyethylene buoy connected by a line and a pulley system to a PTO model, situated on a gantry above the water, see Fig. 1. The buoys have a diameter of 0.488 m, height of 0.280 m, and a total weight of 4378 kg. The PTO model is based on 2 mm thick rotating aluminium discs (40 mm diameter). The linear damping is achieved by eddy current breaks, realized by magnets mounted on the sides of the discs. The details of the PTO set-up and its performance are given in [12].

During the experiment, the position of the floaters in 6 degrees of freedom was measured by an optical system, consisting of eight cameras situated around the basin and reflective markers attached on each buoy. The PTO data (position, velocity, damping values) were acquired or calculated through an Inertia Measurements Unit positioned on the disc, while the damping values were evaluated by measuring the achieved speed at steady state with a known weight. In these experiments, a constant damping value of 306 Ns/m for all the converters was used.

### B. WEC arrays

Three different array layouts have been tested. The arrays have been chosen based on previous simulation results. The array's configurations are obtained by positioning the floaters over a fixed grid of 2 x 2 m wide cells. The locations of the buoys within the three layouts is shown in Fig. 2, and are later on referred as array 1 (A1), array 2 (A2) and array 3 (A3), respectively.

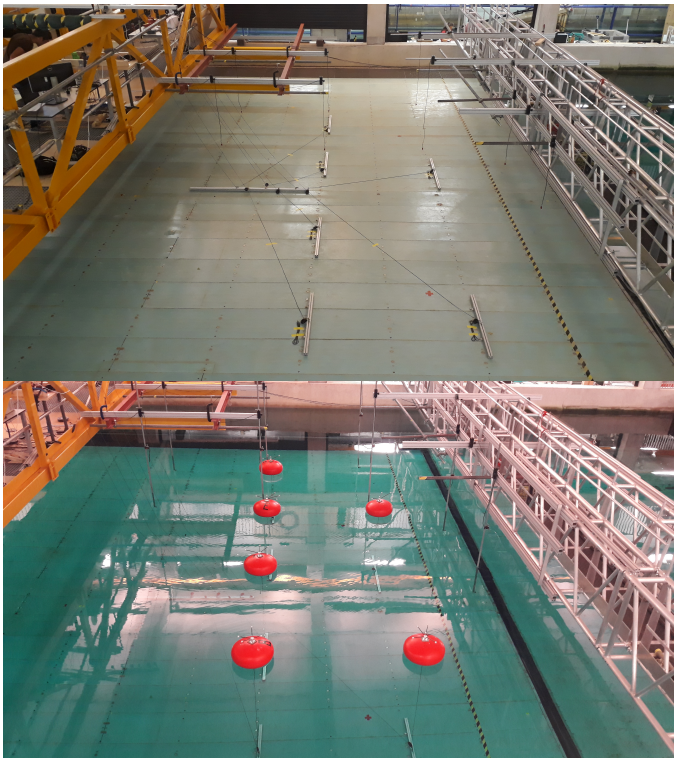

Fig. 1. Picture of one of the arrays in the wave tank (A1). Top: dry setup: attachment bars and ropes connections. Bottom: corresponding setup with filled tank. Each buoy is connected by a line to a power take-off at the gantry above the water.

A1 consists of a two-line array with complete line on the back and a line filled every second spot in the front; A2 consists in a classical 3 line staggered configuration and A3 is a 3 lines aligned array. The array width $D$ is defined as the width of the array perpendicular to the wave direction. The arrays A1-3 have width $D = 6$ m, 6 m, and 2 m, respectively. Each array's upstream line is located at 9.8 m from the wave makers. Layout A1 has been tested twice, while layout A2 and A3 have been tested once.

### C. Wave tank and sea states

The experiments were carried out in the Ocean basin of the COAST laboratory at the University of Plymouth, UK. The wave tank is 35 m long and 15.5 m wide. For these experiments, a water depth of 2.5 m was chosen, corresponding to 25 m in full scale. The waves were reproduced by 24 flap-type paddles, and wave reflection is minimized at the end of the tank by a convex beach. The surface elevation was measured by a set of ten calibrated resistive wave gauges, situated around the WECs as shown in Fig. 2 (G1 to G10). Their location was decided in order to be able to measure the wave elevation at each line of the arrays, as well as the incoming and outgoing waves. All the probes are located on the right side of the tank, in order not to interfere with the optical system used to caption the motion of the buoys.

Five regular and five irregular sea states were studied for each layout, with wave height $H$ and corresponding significant wave height $H_s = \sqrt{2}H$, and wave (energy) periods in the

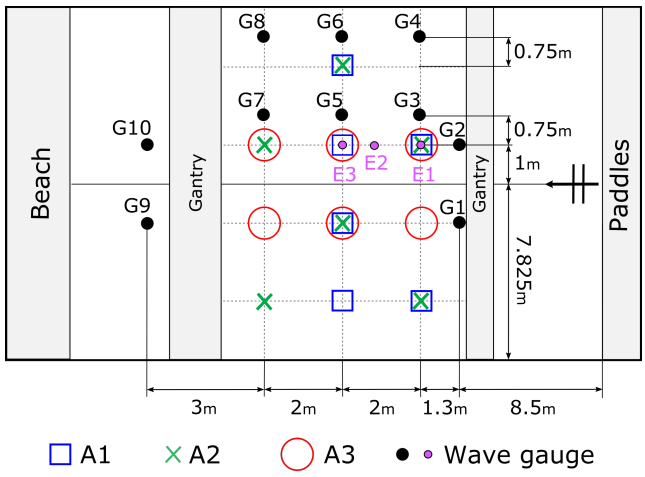


Fig. 2. Schematic view of the wave basin and of the 3 different layouts tested. Different symbols represent the locations of the floaters in 3 distinct configurations (blue squares for array 1 (A1), green cross for array 2 (A2) and red circles for array 3 (A3). G1-10 represent the wave gauges locations and ID; E1-3 represents the wave gauges locations and ID during empty tank tests.

range $1.11-2.37$ s. As such, the five regular and five irregular waves are defined such that they have the same energy per ocean area and energy transport per meter wave crest. The time series of the irregular waves were obtained by a Bretschneider spectrum. The focusing point, i.e. the $x$-coordinate where the input wave elevation of the software is supposed to be recreated, was set to 9.8 m from the wave makers, which corresponds to the front line of each array. The ten target waves are listed in Table I, and the actual waves produced in the tank during the experiments is shown in Figs. 3-4.

Empty tank tests were performed to verify the measurements in different positions within the wave basin. During these tests, the wave elevation was measured by three resistive wave gauges (E1 to E3 in Fig. 2).

## III. Results and Discussion

Understanding the differences between expected and measured wave elevation around the basin is important for simulations' validation and interpretation of the results. Therefore, in this paper experimental results from the wave elevation measurements in the basin is presented, together with results of power transport and power absorption of the three different arrays in irregular waves. The results are obtained only from the analysis of the wave probes data and of the optically acquired buoys' motion data. Power take-off data are not included here.

TABLE I
THE (SIGNIFICANT) WAVE HEIGHTS AND (ENERGY) PERIODS OF THE FIVE REGULAR AND FIVE IRREGULAR WAVES STUDIED.

| | Regular $H = 0.124$ m | Irregular $H_s = 0.175$ m |
|---|---|---|
| $T, T_e = 1.11$ s | RW1 | IW1 |
| $T, T_e = 1.42$ s | RW2 | IW2 |
| $T, T_e = 1.74$ s | RW3 | IW3 |
| $T, T_e = 2.06$ s | RW4 | IW4 |
| $T, T_e = 2.37$ s | RW5 | IW5 |

### A. Wave elevation

The significant wave height $H_s$ and energy period $T_e$ have been computed from the measurement of the surface elevation at the wave gauges; by mean of Fast Fourier Transform (FFT) the spectral density function $\widetilde{S}(f)$ of each measurement elevation series is calculated. Then the $n$-th spectral moments can be calculated as:

$$m_n = \int_0^\infty f^n \widetilde{S}(f)\, \mathrm{d}f, \tag{1}$$

from which the energy period and significant wave height are calculated as

$$T_e = \frac{m_{-1}}{m_0}, \quad H_s = 4\sqrt{m_0} \tag{2}$$

Results have been compared to the expected significant wave height and are shown in Figs. 3-4 for different locations in the wave tank. The comparison with empty tank tests at the same x-coordinate has been also made, which allows some evaluation of the influence of scattered and radiated waves from the floater on the probes measurements. Moreover, A1, A2 and A3 have different symmetries with respect to the center of the tank, the side walls and the wave gauges. It results in different distances between buoys and probes which influence the measured wave elevation. For example, in A1 and A2 the probe G1 has no buoy immediately downstream, while the situation is different for A3. Therefore, some scattering in the result data is expected.

Fig. 3 shows the significant wave height in correspondence of the focusing point, i.e. the first line of the arrays. Results from gauge G3 differs from the one from gauge G4. G3 is located closer to the center of the tank, while G4 is located closer to the right side wall. In all the three different layouts, a floater exists in association with probe G3, while no buoy is found close to G4. Accordingly, results are closer to the empty tank test for G4 (Fig. 3 right). Regarding the second line of the arrays, results are presented in Fig. 4, i.e from G5, G6 and E3. Layout A1 and A2 have different floater locations in this line. It can be noted that layout A3 has the lowest influence on G6, therefore the measurement is very close to the one of the calibration test.

From the results it is clear that, even in the empty tank tests, the expected significant wave heights was never delivered, but always under-reproduced. The discrepancies are larger in correspondence of shorter periods and in the calibration tests. The divergence from the theoretical value of $H_s = 0.175$ m is between 8% to 24%. An error within 10% is within the limits of what is achievable for irregular wave runs without calibration in the experimental wave tank. Lower period runs having higher error, and therefore lower significant wave height, is probably due to wave breaking.

During the array testing the general trend of the wave statistics was clearly reproduced, but, when comparing the different arrays, the spread of the results of the experimental data is related to scattered and radiated waves. The boundaries

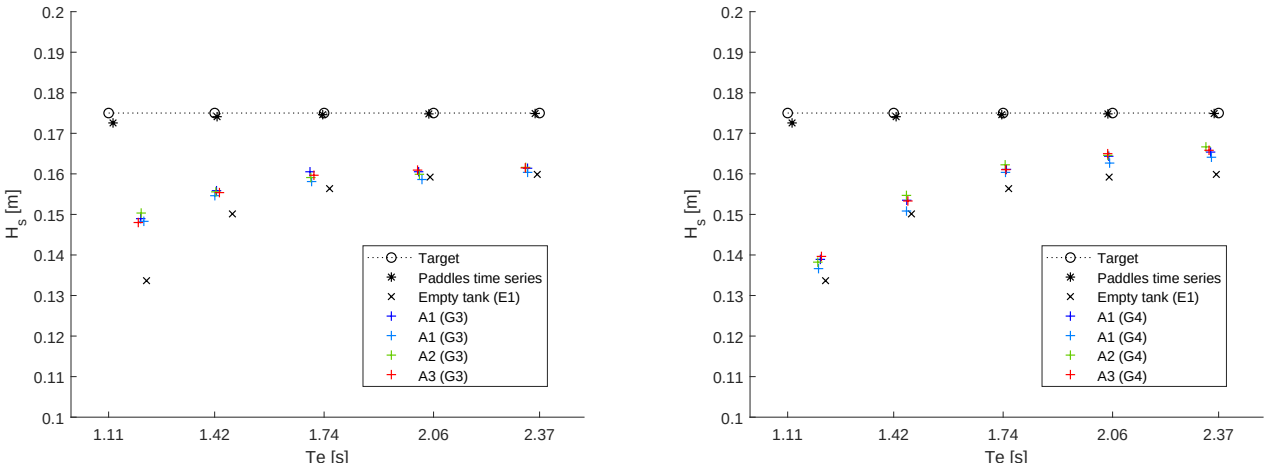


Fig. 3. Comparison between expected significant wave height $H_s$ vs. energy period $T_e$ and measured one in correspondence of the second line of the wave probes (G3 - Fig. on the left and G4 - Fig. on the right). E1 indicate the measurement during the empty tank tests.

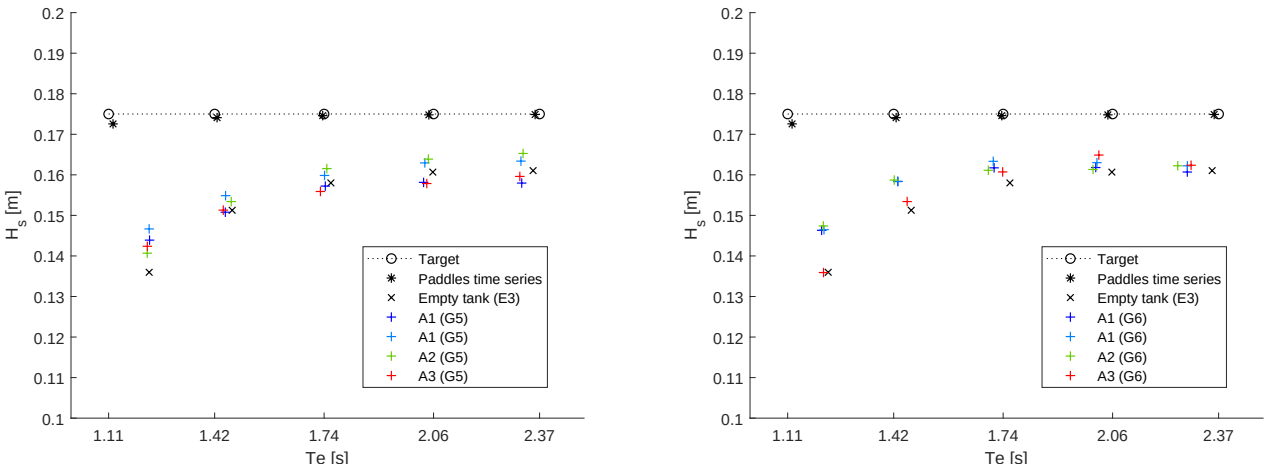


Fig. 4. Comparison between expected significant wave height $H_s$ vs. energy period $T_e$ and measured one in correspondence of the third line of the wave probes (G5 - Fig. on the left and G6 - Fig. on the right). E3 indicate the measurement during the empty tank tests.

influence and the initial water surface condition affect the results as well. Therefore, sometimes the difference in $H_s$ between the two runs with the same layout are larger then between the different layouts. The importance of scattered and radiated waves in the array is also shown from calculation of the percentual wave height reduction after the array, which is quite different between measurements of gauges G1-G9 or G2-G10; for A1 and A3, the $H_s$ reduction varies among the wave periods (Fig. 5). The highest wave height reduction is achieved by array A3, in all wave frequencies. This is expected, since array A3 has three buoys directly after each other in the wave direction, whereas the other two layouts have maximally two. Also, the symmetric layout of array A3 is reproduced in the symmetric results of the wave elevation. Array A2 has a higher wave height reduction between gauges G2 and G10, which is consistent with the presence of two buoys in between the gauges, as compared to only one buoy between gauges G1 and G9. The wave height reduction for array A1 shows a different, asymmetric pattern. The wave height is reduced more along the line of wave gauges G1-G9, than along the line of wave gauges G2-G10. This could possibly be explained by the fact

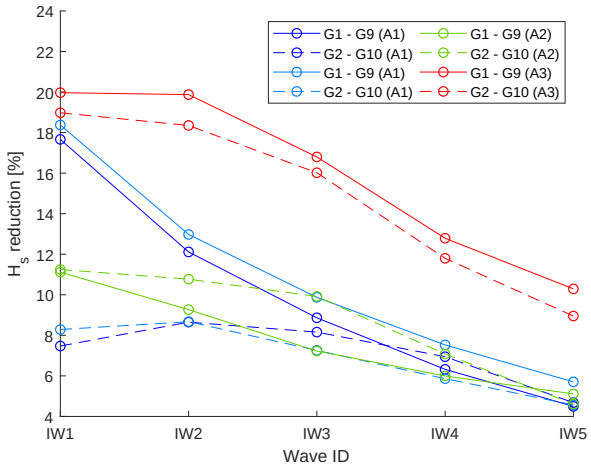


Fig. 5. Significant wave height reduction [%] computed from the surface elevation just before and after the arrays.

that there are five buoys in the three lines closest to G1-G9, whereas only four in the three lines closest to G2-G10. However, a more thorough mapping of the two-dimensional

wave field including all scattered and radiated waves is needed to analyse this in detail.

### *B. Power transport*

The incident and outgoing power transport per meter crest width [W/m] for the WEC array is shown for all irregular waves for arrays A1, A2, and A3 in Figs. 6-8. The power transport has been computed as

$$J = \frac{\rho g^2}{64\pi} H_s^2 T_e \tag{3}$$

from the surface elevation data before and after the array. As can be seen, the power transport per meter wave crest increases for the increasing wave periods. Also, the incident power transport into the WEC array is constantly larger than the outgoing, which shows that energy has been absorbed by the array. The average incoming wave power transport is between 13 and 32 W/m, while the outgoing is between 8 and 28 W/m, according to array and wave period.

The comparison among the arrays is shown in Fig. 9, where the average of the experimental results have been plotted, together with the theoretical power transport, the one programmed in the paddles software and the one calculated from the calibration tests (at gauges E1). $J_{\text{in}}$ and $J_{\text{out}}$ includes also the back-scattered and radiated waves; the calibration tests shows that the actual incoming power is lower than the theoretical and the measured one during the array tests. As thus, $J_{\text{in}}$ does not really represent the incident power transport in the waves produced by the wave tank paddles, but is the power transport just before the array, including the wave field produced by the array. As a comparison, the undisturbed incident power transport has been computed from the surface elevation in the empty tank tests, and is referred to as $J_0$.

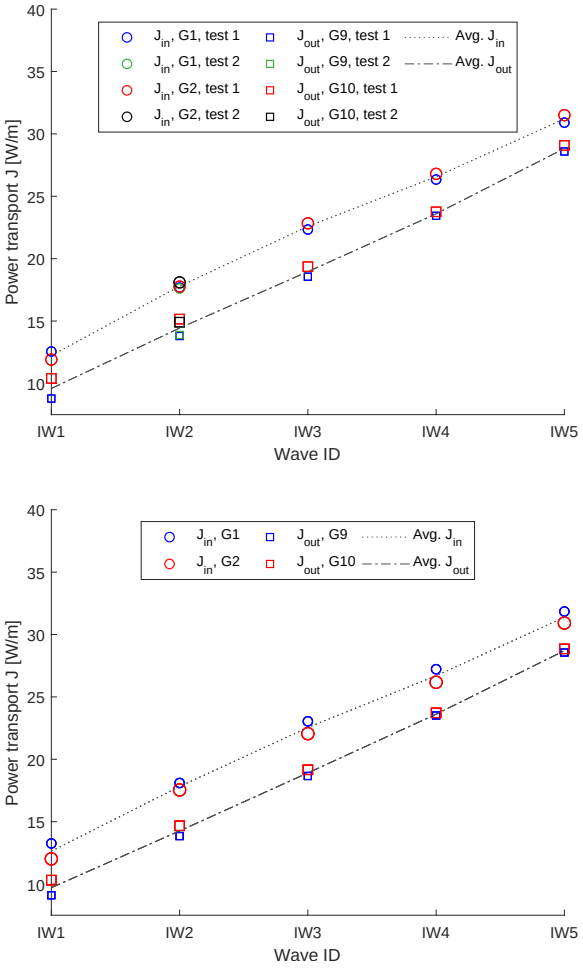


Fig. 6. Incident and outgoing power transport per meter wave front for array A1 first run (top) and second run (bottom) for all the irregular waves tested. As the tests have been repeated, several markers are shown for each test. The average trend is shown by the lines.

### *C. Power absorption*

Figs. 10-11 show the energy absorption of arrays A1, A2, and A3. The absorption is analysed by means of two methods: directly by computing the absorption from the buoys' motion, and indirectly by comparing the available wave power before and after each array.

*1) Power absorption from the buoy motion:* the buoy dynamics in the three translational degrees of freedom,

$$\bar{x}(t) = \sqrt{x(t)^2 + y(t)^2 + (h + z(t))^2} \tag{4}$$

has been analysed and the absorbed power computed from the velocity,

$$P^{\text{i}}_{\text{abs}}(t) = \gamma\, \dot{\bar{x}}(t)^2, \tag{5}$$

where $\gamma$ is the constant damping of the power take-off, $h$ is the water depth. The absorbed power shown in the figure is the sum of all six buoys' time-averaged value of the instant absorbed power in Eq. (5),

$$P^{\text{array}}_{\text{abs}} = \sum_{i=1}^{6} \bar{P}_i(t). \tag{6}$$

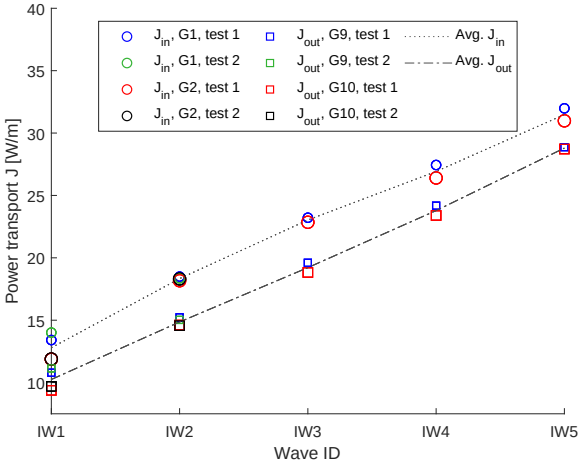


Fig. 7. Incident and outgoing power transport per meter wave front for array A2 for all the irregular waves tested. As the tests have been repeated, several markers are shown for each test. The average trend is shown by the lines.

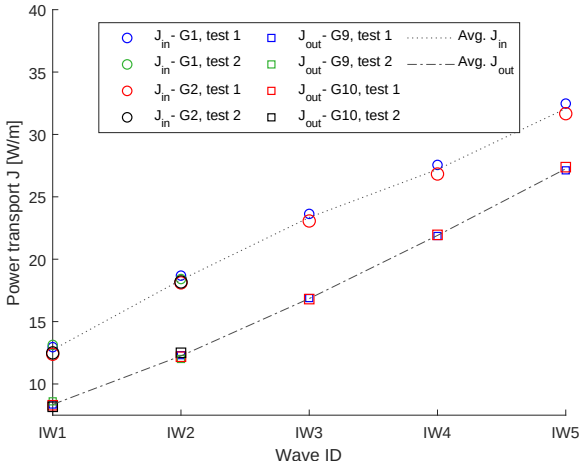


Fig. 8. Incident and outgoing power transport per meter wave front for array A3 for all the irregular waves tested. As the tests have been repeated, several markers are shown for each test. The average trend is shown by the lines.

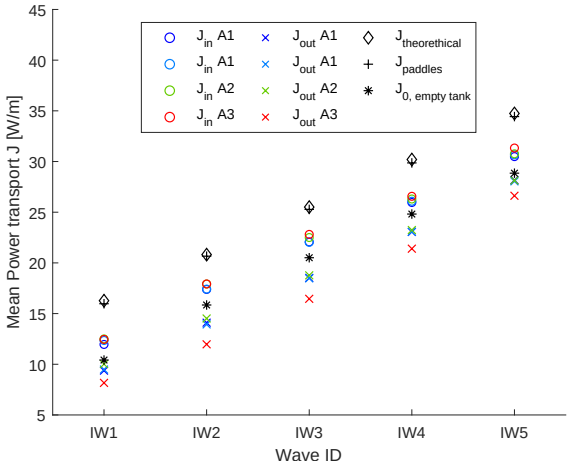


Fig. 9. Comparison of average incoming and outgoing power transport for all the arrays tested. The average is taken over measurements of gauges G1 - G2 for $J_{\text{in}}$ and gauges G9 - G10 for $J_{\text{out}}$. If more tests were executed, the average over all the tests was taken as well. $J_{\text{theorethical}}$ is computed from the target values of $H_s$, $T_e$; $J_{\text{paddles}}$ is computed from the programmed paddle input and $J_0$ is computed from empty tank test measurements at gauge E1.

*2) Power difference from the surface elevation:* from the wave gauges situated before and after the array in the wave direction, the power in the waves incident into and outgoing from the array has been analysed, similarly as the power transport analysed above. From the surface elevation, the spectrum and spectral moments have been computed as in Eq. (1). The incident time-averaged power into the array is computed as $J_{\text{in}} \cdot D$ [W], where $D$ is the array width defined previously and $J_{\text{in}}$ the incident power transport per meter crest width computed according to Eq. (3), with significant wave height and energy period computed as in Eq. (2) from the surface elevation just before the array. Likewise, the outgoing time-averaged power from the array is computed as $J_{\text{out}} \cdot D$ [W], with wave parameters evaluated at the wave gauges after the array. The array width, i.e. the distance, perpendicular to the wave front, between the two most distant buoys of an array, is $D = 6$ m, 6 m and 2 m for arrays A1-3. The time-averaged power difference between the incident and outgoing available wave power is

$$P_{\text{diff}}^{(\text{b})} = (J_{\text{in}} - J_{\text{out}}) \cdot D. \tag{7}$$

For comparison, the power difference has been also computed as

$$P_{\text{diff}}^{(\text{c})} = (J_0 - J_{\text{out}}) \cdot D, \tag{8}$$

where $J_0$ is the undisturbed incoming power per meter of crest front, i.e. without the influence of scattered and radiated waves, and $J_{\text{out}}$ as before, calculated from the gauges after the array.

The power absorption computed by the two methods is shown in Figs. 10-11; Fig. 10 with the incident power transport including the wave field produced by the array, i.e. using Eq. (7), and Fig. 11 with the undisturbed incident power transport, using Eq. (8).

In Fig. 10, it can be seen that both methods give the same trend in the power absorption, but the averaged absorbed power by the array is lower than the difference in energy going into and coming out from the array, as computed from the surface elevation including the back-scattered and radiated waves. If, instead, the undisturbed incident power transport $J_0$ is used and the difference in wave power before and after the array is computed as in Eq. 8, a better agreement between the two methods is observed, as seen in Fig. 11.

It can be seen from the figures that array A3 has the lowest power absorption among the arrays, whereas array A1 and A2 have comparable power absorption. Thus, array A3 both has the largest percentual wave height reduction (see Fig. 5) and the lowest power absorption. This is in no contradiction, as the total incident wave power available to array A3 is lower than for arrays A1-2, due to the smaller array width. In fact, due to the shadowing effect, both a lower power absorption and a larger wave height reduction should be expected for array A3, which is also seen in the experimental results.

The total absorbed power from the floater dynamics, which includes all the translational and rotation degree of freedom, reach its maximum for IW4 for all the arrays, with a total of around 11 Watts.

To analyse the performance of the arrays further, the power absorption of the individual WECs is also studied. Figs. 13-15 show the power absorption of the 6 buoys (called A, B, C, D, E, F) for the different arrays, calculated as in Eq. (5). The relative buoy location during the tests is shown in Fig. 12.

Generally, each buoy absorbs between 0.5 W and 2.5 W, depending on the array, the wave condition and relative location within the layout. Fig. 13 shows that buoys A and D, located in the front line of array A1, have similar power absorption; buoys B and E are the two shadowed floats and produce the lower power. The highest motion is achieved by buoy C, followed by buoy F. The array is not fully symmetric; despite the similar behaviour of some of the buoys, there is visible asymmetric behaviour.

Fig. 14 shows the power of the buoys within A2. The behaviour of the buoys within the staggered layout is highly dependent on the wave period.

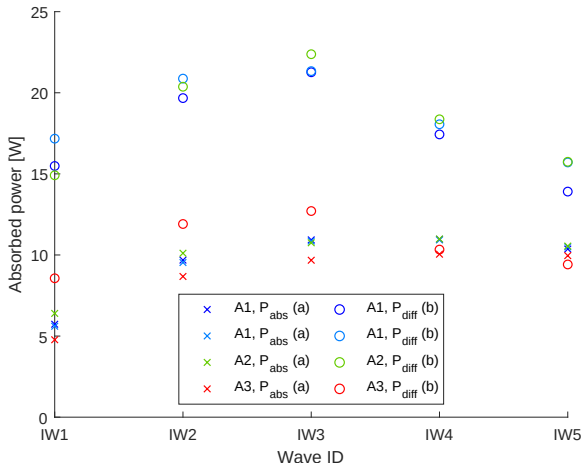


Fig. 10. Comparison between the power absorption derived from the buoy motion (a) and the power difference between incident and outgoing wave energy, computed from the surface elevation at the wave gauges before and after the array as in Eq. 7 (b). In this latter case, the power transport is computed as the difference between the average over measurements of gauges G1 & G2 for $J_{\text{in}}$ and gauges G9 & G10 for $J_{\text{out}}$. If more tests were executed, the average over all the tests was taken as well.

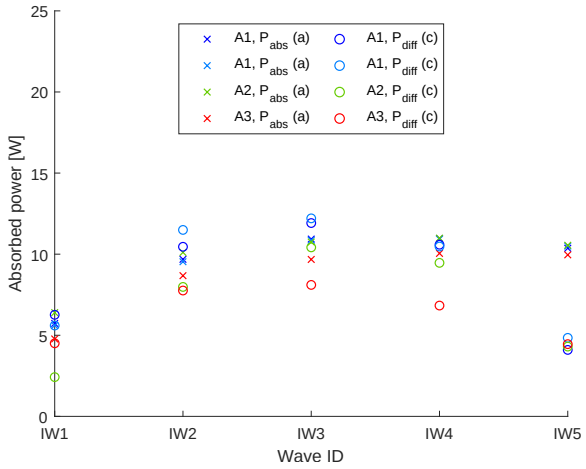


Fig. 11. Comparison between the power absorption derived from the buoy motion (a) and the power difference between incident and outgoing wave energy, computed from the surface elevation at the wave gauges before and after the array as in Eq. 8 (c). In this latter case, the power transport is computed as the difference between the empty tank test power transport $J_0$ and the average over measurements of gauges G9 & G10 for $J_{\text{out}}$. If more tests were executed, the average over all the tests was taken as well.

Array A3 is shown in Fig. 15. The WECs in the front line (buoy A and D) absorb much power whereas the WECs in the back (buoy B and F) absorb less. The WECs in the middle line, however, show an asymmetric behaviour: buoy C absorbs more power than buoy E. The asymmetric behaviour is reflected in the $H_s$ reduction, where the side of the array with the higher motion, and the highest power absorption, has the highest wave reduction (i.e. between gauges G1-G9).

## IV. Conclusions

The paper has presented wave tank experiments of wave power arrays with six point-absorber devices. Each wave energy converter consists of a floating ellipsoid buoy moving in six degrees of freedom and connected to an individual power

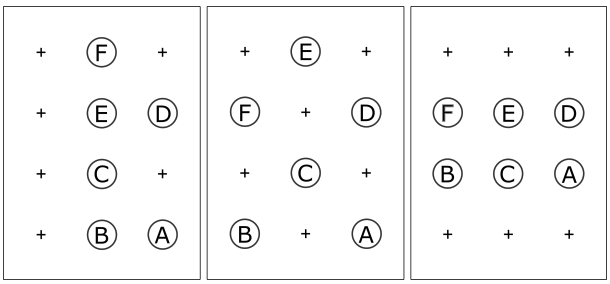


Fig. 12. Outline of the floater locations within the different arrays.

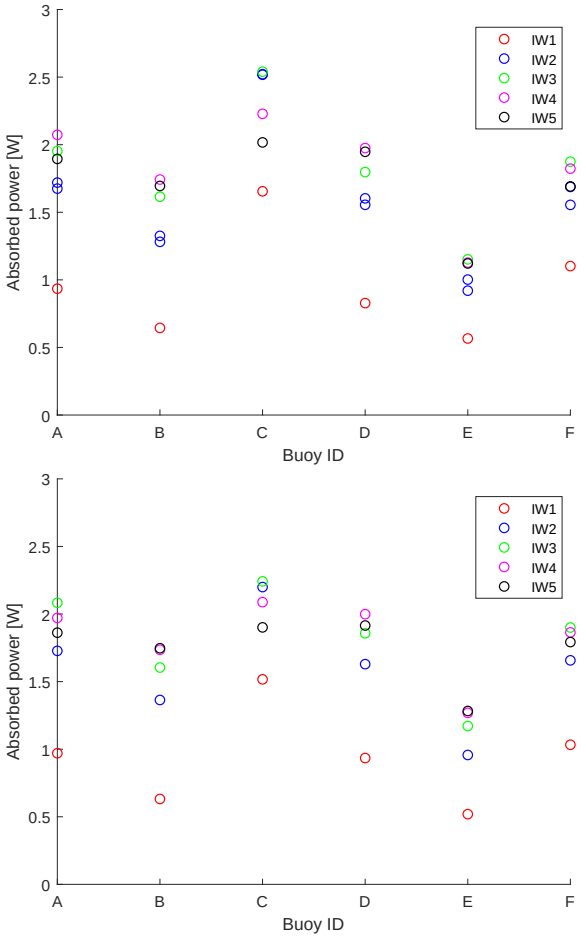


Fig. 13. Power absorption derived from the buoy motion (Eq. 5) for the different buoys of layout A1 (first run, top - second run, bottom).

take-off. Three different array layouts have been tested and compared.

The power transport has been computed from the surface elevation before and after the arrays. The power transport increases with increasing energy period, and in all arrays and waves, there is a clear reduction of the power transport after the array.

Two different methods have been employed to analyse the power absorption of the arrays. In the direct method, the power absorption has been computed from the buoy dynamics, with absorbed power equal to the power take-off damping times the velocity of the buoy squared. In the indirect method, the difference between the wave power available before and after

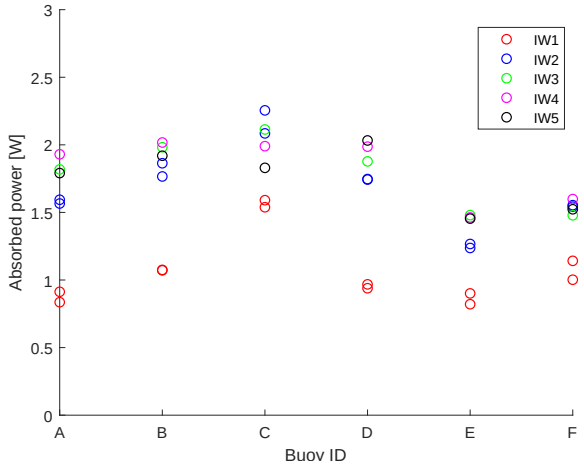


Fig. 14. Power absorption derived from the buoy motion (Eq. 5) for the different buoys of layout A2.

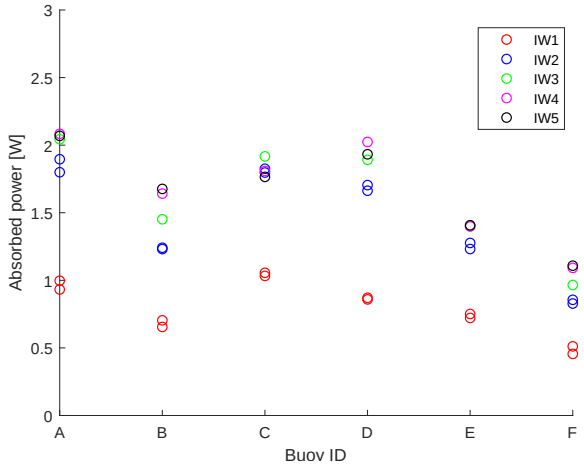


Fig. 15. Power absorption derived from the buoy motion (Eq. 5) for the different buoys of layout A3.

the array has been analysed. The presence of the connection line between the buoy and the PTO induce in the system non linear behaviour, so that the buoy motion cannot be assumed a priori equal to the PTO motion. As such, the direct method of power absorption calculation from the buoy motion is a first estimation and can be different from the real absorbed power from the PTO.

The largest percentage reduction in wave height before and after the array is obtained the array A3, which has most buoys directly situated after each other in the wave direction. In other words, shadowing effect is largest in this array, which is to be expected. This also implies that the power absorption of array A3 is lower than for the other two arrays, which is also shown by the experimental results obtained by both methods.

Arrays A1 and A2 have similar mean wave elevation reduction, as well as power absorption.

The analysis of the incoming wave data has highlighted the main uncertainties and deviations of the incoming waves into the arrays from the expected ones. The behaviour of the specific buoys in each array has been also presented. The power absorption of the single buoys has shown an non symmetric behaviour, even in the symmetric configuration, due to disturbances propagation in the tank.

The results presented in this paper will serve as input for further comparison between simulation results, power absorption from buoys motion and power absorption from the PTOs.

## REFERENCES

[1] M. Leijon, R. Waters, M. Rahm, O. Svensson, C. Boström, E. Strömstedt, J. Engström, S. Tyrberg, A. Savin, H. Gravråkmo *et al.*, "Catch the wave to electricity: the conversion of wave motions to electricity using a grid-oriented approach," *IEEE Power and Energy Magazine*, vol. 7, no. 1, pp. 50–54, 2009.

[2] M. Göteman, J. Engström, M. Eriksson, J. Isberg, and M. Leijon, "Methods of reducing power fluctuations in wave energy parks," *Journal of Renewable and Sustainable Energy*, vol. 6, no. 4, p. 043103, 2014.

[3] E. Mackay, J. Cruz, M. Livingstone, and P. Arnold, "Validation of a time-domain modelling tool for wave energy converter arrays," *EWTEC 2013*, 2013.

[4] D. N. Konispoliatis and S. A. Mavrakos, "Mean drift loads on arrays of free floating owc devices consisting of concentric cylinders," in *Proceedings of the 29th International Workshop on Water Waves and Floating Bodies (IWWWFB2014)*, 2014.

[5] F. C. da Fonseca, R. Gomes, J. Henriques, L. Gato, and A. Falcao, "Model testing of an oscillating water column spar-buoy wave energy converter isolated and in array: Motions and mooring forces," *Energy*, vol. 112, pp. 1207–1218, 2016.

[6] P. Mercadé Ruiz, F. Ferri, and J. P. Kofoed, "Experimental validation of a wave energy converter array hydrodynamics tool," *Sustainability*, vol. 9, no. 1, p. 115, 2017.

[7] P. Troch, V. Stratigaki, T. Stallard, D. Forehand, M. Folley, J. Kofoed, M. Benoit, A. Babarit, D. G. Sánchez, L. Bosscher *et al.*, "Physical modelling of an array of 25 heaving wave energy converters to quantify variation of response and wave conditions," in *Proceedings the 10th European Wave and Tidal Energy Conference Series (EWTEC), Aalborg, Denmark*, 2013, pp. 2–5.

[8] V. Stratigaki, P. Troch, T. Stallard, D. Forehand, J. P. Kofoed, M. Folley, M. Benoit, A. Babarit, and J. Kirkegaard, "Wave basin experiments with large wave energy converter arrays to study interactions between the converters and effects on other users in the sea and the coastal area," *Energies*, vol. 7, no. 2, pp. 701–734, 2014.

[9] V. Stratigaki, P. Troch, T. Stallard, D. Forehand, M. Folley, J. P. Kofoed, M. Benoit, A. Babarit, M. Vantorre, and J. Kirkegaard, "Sea-state modification and heaving float interaction factors from physical modelling of arrays of wave energy converters," *Journal of Renewable and Sustainable Energy*, vol. 7, no. 6, p. 061705, 2015.

[10] B. Child and P. L. Weywada, "Verification and validation of a wave farm planning tool," in *Proceedings of the 10th European Wave and Tidal Energy Conference (EWTEC) conference, Aalborg, Denmark*, 2013, pp. 2–5.

[11] M. Giassi and M. Göteman, "Layout design of wave energy parks by a genetic algorithm," *Ocean Engineering*, vol. 154, pp. 252–261, 2018.

[12] S. Thomas, M. Giassi, M. Göteman, M. Hann, E. Ransley, J. Isberg, and J. Engström, "Performance of a direct-driven wave energy point absorber with high inertia rotatory power take-off," *Energies*, vol. 11, no. 9, p. 2332, 2018.